ACS Catalysis

Research Article

pubs.acs.org/acscatalysis

Synthesis of Carbon Nitride Semiconductors in Sulfur Flux for Water Photoredox Catalysis

Jinshui Zhang, Mingwen Zhang, Guigang Zhang, and Xinchen Wang*

Research Institute of Photocatalysis, Fujian Provincial Key Laboratory of Photocatalysis−State Key Laboratory Breeding Base, Fuzhou University, Fuzhou 350002, P. R. China

ABSTRACT: Sulfur-mediated synthesis has been demonstrated as a simple but efficient pathway to control the texture and electronic structure of poly(tris-triazine) based graphitic carbon nitride semiconductors with improved photocatalytic reactivity over the pristine counterpart. Here, we advance this strategy by employing cheap and easily available elemental sulfur as the external sulfur species instead of sulfur-containing precursors for the sulfur-mediated synthesis of polymeric carbon nitride photocatalysts. Characterization results revealed that the multiple thermal condensations of carbon nitride precursors in the hot sulfur flux provided a facile means to promote the formation of graphitic-like carbon nitride conjugated systems, altering the traditional route of thermal-induced self-polymerization of melamine. The textural, electronic, and optical properties of the resultants organic semiconductors was therefore strongly modified to endow the materials with improved physical and chemical properties, as demonstrated by the enhanced photocatalytic activity for water reduction and oxidation under visible light irradiation with wavelength >420 nm. This result again underlines the benefit of a sulfur-mediated approach to construct and manipulate polymeric carbon nitride networks for sustainable applications in catalysis and photocatalysis.

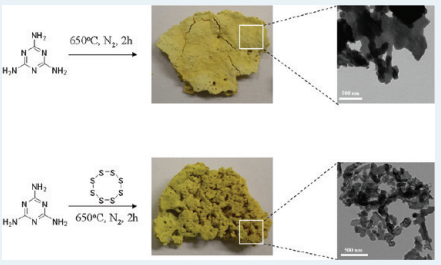

KEYWORDS: *carbon nitride, elemental sulfur, sulfur-mediated synthesis, solar energy conversion, photocatalysis*

1. INTRODUCTION

The search for renewable energy resources has gained worldwide attention nowadays, due to the increasing concerns for energy and environment issues.[1−5] The sun is the ultimate source of energy of fossil fuels and all living things, which has for a long-time been considered as idea future energy resource, provided that it can be captured, converted, and stored in a sustainable manner.[6,7] In recent years, there has been a burst of activity on solar energy utilization by converting sunlight to heat, electricity, chemical fuel, and so on.[8,9] Among these, splitting water by sunlight via charge generation, separation, and subsequent redox reactions on a semiconductor to produce hydrogen gas is attracting renewed attention, because hydrogen is a clean, infinite, and the lightest chemical fuel and, for example, can be applied in fuel cells to generate electricity.[10−17] Since the report of water splitting in the Pt/TiO_2 photoelectrochemical cell by Fujishima and Honda in 1972,[18] countless efforts have been directed to establish stable light-harvesting systems for water splitting, while still investigating natural photosynthesis as an inspiration for artificial one.[19−30] Significant advances in homogeneous and heterogeneous photocatalysis have been made during the past 40 years; however, the process has still been limited by antenna substances that are required to be nontoxic, inexpensive, stable, efficient, and earth-abundant as well as can harvest visible spectrum to run the chemical reactions.[31]

Binary carbon nitride solids, a valuable extension of carbon materials, has attracted worldwide renaissance attention since the diamond-like β-C_3N_4 was predicted by Cohen and his co-workers.[32] Theoretical studies demonstrate that there are several allotropes presented in covalent carbon nitride materials, such as α, β, cubic, pseudocubic, and graphitic phases.[33] Among various allotropes, graphitic carbon nitride (g-C_3N_4) is the most stable phase under ambient conditions and has the smallest semiconductor band gap (<3 eV) due to the sp^2 hybridization of carbon and nitrogen, forming a stable, extended π-conjugated system.[34] Owing to its unique electronic features, g-C_3N_4 was recently introduced as a metal-free visible light photocatalyst for water reduction/oxidation in the presence of electron donor/acceptor.[34] The photocatalytic activities of g-C_3N_4 can be enhanced by loading with cocatalysts, such as Pt, Pd, Au,[35,36] RuO_2, and Co_3O_4.[35,37] In addition, much effort was devoted to modifying the intrinsic properties of g-C_3N_4 to advance its photocatalytic activity with both inorganic and organic protocols. Many strategies have been developed, e.g. doping with metal/nonmetal elements,[38−43] protonation with HCl,[44] dye sensitizing,[45] nanostructuring,[46−49] copolymerization,[50,51] and hybridization.[52−54] Our recent work demonstrated that using sulfur-containing organic and inorganic compounds, such as trithiocyanuric acid (TA),[55] ammonium thiocyanate (AT),[56] or thiourea (TU)[57] as the precursors can produce g-C_3N_4 photocatalysts, and the presence of sulfur motifs can provide an extra chemical way to control condensation/polymerization of g-C_3N_4 due to the

Received: March 12, 2012
Revised: April 18, 2012
Published: April 18, 2012

involvement of easy leaving groups such as −SH. This sulfur-mediated approach offers a simple, but efficient pathway for the synthesis of g-C_3N_4, and we believe that further development of this synthetic approach will find much utility in fabrication of advanced carbon nitride materials for energy-related applications, especially for water photoredox catalysis because the band gaps of the polyheptazine semiconductor straddle water reduction and oxidation potentials.

Elemental sulfur, an abundant bright yellow crystalline solid, is widely used in chemistry laboratory and industry. For instance, it can be used as the starting material for sulfuric acid production, a central substance in the chemical industry, whose principal usages including lead-acid batteries for cars and other vehicles, ore processing, fertilizer manufacturing, oil refining, wastewater processing, and chemical synthesis.[58] Recently, elemental sulfur has been extensively used in the synthesis of inorganic materials owing to its unique physical properties (e.g., low melting point at 115.2 °C and moderate boiling point at 444.6 °C) and multivalent redox properties (either as an oxidant or reducing agent).[59−62] Helton et al. used elemental sulfur to react with copper(I) complexes, providing an excellent starting point for investigations on Cu−S chemistry.[63] Yin et al. introduced it as an oxidizing species in a colloidal solution to generate cobalt sulfide hollow nanocrystals.[64,65] Elemental sulfur can also be activated by octadecene to control the formation of CdS nanocrystals, developing a noninjection synthesis method for high-quality CdS nanocrystals.[66] Very recently, Chung et al. demonstrated that elemental sulfur can be directly used as a solvent and reactive medium for the formation of gold nanoparticles and for in situ cross-linking of these colloidal dispersions to form vulcanized nanocomposites.[67]

The wide temperature window (115.2−444.6 °C) of liquid sulfur flux can in principle enable its implementation in polymer synthesis as a solvent medium, for example to promote the mass transfer of bulk condensation of carbon nitride, which is regarded as a major kinetic barrier for the carbon nitride synthesis in the bulk system.[68] Chemically, the deamination process of carbon nitride condensation can also be accelerated by the redox disproportionation process of sulfur with the formed ammonia as described by the eq 1.[69] Importantly, all sulfur species can be facially removed by increasing the reaction temperature to 550 °C in the air, where the graphitic carbon nitride network has been well-known to be extremely stable against thermal attack in the air (up to 600 °C). This makes elemental sulfur a feasible choice as a solvent as well as a chemical promoter for carbon nitride synthesis.

$$10S + 4NH_3 \rightarrow S_4N^- + S_6^{2-} + 3NH_4^+ \quad (1)$$

In this paper, elemental sulfur (S_8) was employed for the first time as the solvent and mediator to promote the chemical synthesis of polymeric g-C_3N_4 photocatalysts from melamine via a thermal-induced self-condensation process. The resultant g-C_3N_4 catalysts were subjected to several characterizations to study the influence of the hot sulfur flux synthesis on their texture, morphology, optical, and electronic properties. The photocatalytic activity of g-C_3N_4 for water reduction and oxidation reactions driven by visible light irradiation was also described.

2. EXPERIMENTAL METHODS

2.1. Materials. Melamine (99%) was purchased from Alfa Aesar. Elemental sulfur (S_8, 99.5%), triethanolamine (99%), and chloroplatinic acid hexahydrate ($H_2PtCl_6{\cdot}6H_2O$, ≥37.5% Pt basis) were obtained from Sigma-Aldrich. All chemicals were used as received, without further purification.

2.2. Synthesis Procedure. A 3 g portion of melamine was first mixed with a certain amount of S_8 (1, 2, 3, 5, or 10 g) and well ground in an agate grinding at least 40 min. Then, the mixture was transfer into a crucible with cover and heated directly in N_2 flow at 650 °C for 2 h. The resultant samples were denoted as CN-S_x, where x refers to the amount of S_8, e.g. CN-$S_{2.0}$. The sample obtained by simply heating melamine at 650 °C was denoted as CN and was used as a reference sample.

2.3. Fabrication of Carbon Nitride Electrode. Powder CN and CN-S_x were made as film electrodes on fluorine doped tin oxide (FTO) glass.[50,51] First, FTO glass was cleaned by sonication in chloroform, acetone, and ethanol for 30 min, respectively. The fresh prepared glass was then rinsed with Millipore water and kept in isopropanol for 24 h. A 50 mg portion of powder catalyst was mixed with 2 mL dimethylformamide under sonication for 30 min to get slurry. The slurry was spreading onto FTO glass whose side part was previously protected using Scotch tape. After air-drying, the electrode was fired at 350 °C for 30 min in air to improve adhesion. A copper wire was connected to the side part of the FTO glass using a conductive tape. Uncoated parts of the electrode were isolated with epoxy resin, and the exposed area of the electrode was 0.25 cm^2.

2.4. Characterization. Thermogravimetric analysis (TGA) was performed on TG209 (NETZSCH Co.). Sample pictures were taken by Nikon D3100. Transmission electron microscopies (TEM) were operated by Zeis 912 microscope and JEOL mode JEM 2010 EX instrument. Nitrogen adsorption−desorption isotherms were collected at 77 K using Micromeritics ASAP 2020 surface area and porosity analyzer. Powder X-ray diffraction (XRD) measurements were performed on Bruker D8 Advance diffractometer with Cu Kα_1 radiation (λ = 1.5406 Å). Fourier transformed infrared (FTIR) spectra were recorded on BioRad FTS 6000 spectrometer. X-ray photoelectron spectroscopy (XPS) data were obtained on Thermo ESCALAB250 instrument with a monochromatized Al Kα line source (200 W). Electron paramagnetic resonance (EPR) measurements were carried out at a Bruker model A300 spectrometer. UV−vis diffuse reflectance spectra (DRS) were performed on Varian Cary 500 Scan UV−visible system. Photoluminescence spectra were recorded on an Edinburgh FI/FSTCSPC 920 spectrophotometer. Electrochemical measurements were conducted with a BAS Epsilon Electrochemical System in a conventional three electrode cell, using a Pt plate as the counter electrode and Ag/AgCl electrode (3 M KCl) as the reference electrode. Elemental analysis (EA) results were collected from a Vario MICRO.

2.5. Photocatalytic Activity for Water Splitting. Reactions were carried in a Pyrex top-irradiation reaction vessel connected to a glass closed gas system. H_2 production was performed by dispersing 50 mg of catalyst in an aqueous solution (100 mL) containing triethanolamine (10 vol %) as a sacrificial electron donor. A 3 wt % portion of Pt was loaded on the surface of carbon nitride sample by the in situ photodeposition method using chloroplatinic acid hexahydrate ($H_2PtCl_6{\cdot}6H_2O$). O_2 evolution was carried out by dispersing

dx.doi.org/10.1021/cs300167b | ACS Catal. 2012, 2, 940−948

50 mg carbon nitride in 100 mL aqueous solution containing $AgNO_3$ (0.01M) as the electron acceptor and La_2O_3 (0.2 g) as the pH buffer agent (pH 8.6).[15,70,71] The reaction solution was evacuated several times to remove air completely prior to irradiation under a 300 W xeon-lamp and a water filter. The wavelength of the incident light for H_2 evolution and O_2 evolution was controlled as $\lambda > 420$ nm and $\lambda > 350$ nm with the aid of cutoff filters, respectively. The temperature of the reaction solution was maintained at room temperature by a flow of cooling water during the reaction. The evolved gases were analyzed by gas chromatography equipped with a thermal conductive detector (TCD) and a 5 Å molecular sieve column, using Argon as the carrier gas.

3. RESULTS AND DISCUSSION

The morphology of CN-S_x presents lots of visible channels within the bulk structure as shown in Figure 1, which is

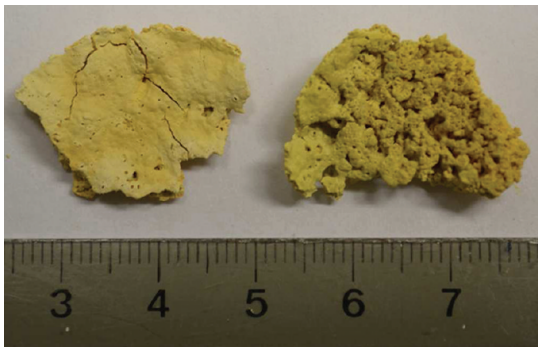

Figure 1. Photograph of the as-prepared CN (left) and CN-$S_{2.0}$ (right).

distinctly different from that of pristine CN. This particular morphology for CN-S_x could be attributed to the mediated effect of the sulfur flux. During the synthesis procedure, when temperature reached to >115.2 °C, S_8 powder melted into liquid, functionalizing not only as the solvothermal solvent to promote molecular diffusion but as the reactant to accelerate the deamination process of carbon nitride condensation by reacting with the produced ammonia. Further increasing temperature above 444.6 °C caused the boiling of the sulfur liquid, giving rise to the formation of sulfur-containing gases acting as inflating medium. Thus, the volatilization of elemental sulfur during carbon nitride polymerization creates lots of pore channels in the bulk structure of CN-S_x. This morphology change on the macroscale (mm) is an indication of the texture evolution in nanoscale (nm), as confirmed by the TEM images in Figure 2. Heating melamine in the absence of elemental sulfur resulted in CN, but with big and smooth layer sheets (Figure 2a). However, by mediating with the S_8 flux, these big g-C_3N_4 sheets are shredded into smaller ones, showing thin sheets in 100−300 nm with some backfolded at the edges (Figure 2b). This suggests that the connectivity and packing of conjugated aromatic systems is strongly modified by the sulfur flux. The corresponding specific surface area (S_{BET}) of CN-S_x is larger than that of pristine CN, owing to its smaller particle size.[46−49] S_{BET} of CN-$S_{2.0}$ is 26 $m^2 \cdot g^{-1}$ that is ca. 3 times higher than that (9 $m^2 \cdot g^{-1}$) of CN (Table 1). The enlarged surface area not only facilitates mass transfer but also provides more activity sites for surface-dependent reactions, being regarded to

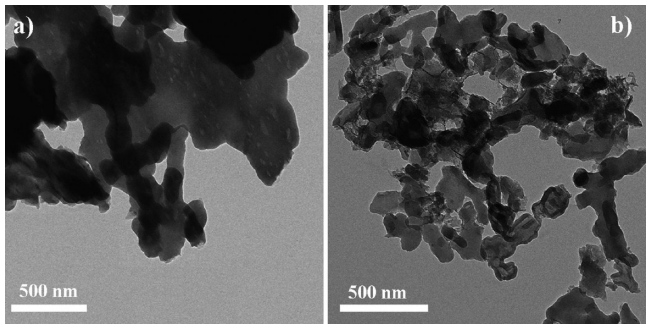

Figure 2. Typical TEM images of CN (a) and CN-$S_{2.0}$ (b).

Table 1. Physicochemical Properties and Photocatalytic Activity of CN and CN-S_x for Hydrogen Evolution with Visible Light ($\lambda > 420$ nm)

catalyst	C/N atomic	[a]S_{BET} $m^2 \cdot g^{-1}$	[b]band gap eV	[c]HER $\mu mol \cdot h^{-1}$
CN	0.73	9	2.76	7.20
CN-$S_{1.0}$	0.72	18	2.69	26.2
CN-$S_{2.0}$	0.71	26	2.65	32.5
CN-$S_{3.0}$	0.71	25	2.64	19.8
CN-$S_{5.0}$	0.71	30	2.61	17.6
CN-$S_{10.0}$	0.70	35	2.58	10.3

[a]Calculated from nitrogen adsorption−desorption isotherms. [b]Estimated from optical measurements. [c]H_2 evolution rate.

promote the photocatalytic redox functions of semiconductive carbon nitride polymers.[46]

Figure 3 shows the XRD patterns of CN-S_x and CN as a reference sample. A highly resembled structure is detected between CN-S_x and CN, with the arising of peaks (002) and (100) at ~27.2° and ~13.0°, respectively.[34,50,51] The intensity of XRD patterns for CN-S_x samples is found to be lower than that of unmodified CN, indicating the increased disturbance of graphitic-like structure caused by the sulfur flux synthesis.[5,51,55] There is a slight shift of the peak (002) from 27.5° for pristine CN to 27.2° for CN-S_x, whereas the peak (100) remains unchanged at 13.0°. It is known that the peak (002) originates from the interlayer reflection of a graphitic-like structure, while the peak (100) is related to the in-plane structural repeating motifs of the aromatic systems.[34,50,51,68] So, the shifting of XRD peak can provide us the information about the structure change as a result of the sulfur flux annealing. According to Bragg's law, the down-shift of peak (002) corresponds to the increasing of interlayer distance from $d = 0.325$ nm for CN to $d = 0.328$ nm for CN-S_x, indicating the slightly loosened packing of the conjugated systems.[34] The void-to-void distance of in-plane structure repeating motifs is determined as $d = 0.681$ nm for CN and CN-S_x on the basis of peak (100) at 13.0°, which is different from the results of TA-derived g-C_3N_4.[55] Our previous work demonstrated that using TA as a precursor for g-C_3N_4 synthesis caused the down-shift of peak (002) and the upshift of peak (100), evidently modifying the structure of the resulting g-C_3N_4 polymers owing to the presence of structured sulfur in TA molecule.[55]

FTIR spectra were performed for the investigation of chemical structure of CN-S_x samples. With the successful evolution of poly(tri-*s*-triazine)-based π-conjugated systems in the sulfur flux, all characteristic vibration bonds assigned to polymeric g-C_3N_4 are clearly seen for CN-S_x samples in Figure 4.[34,50,51,68] For example, the pronounced absorption in 1200−

dx.doi.org/10.1021/cs300167b | ACS Catal. 2012, 2, 940−948

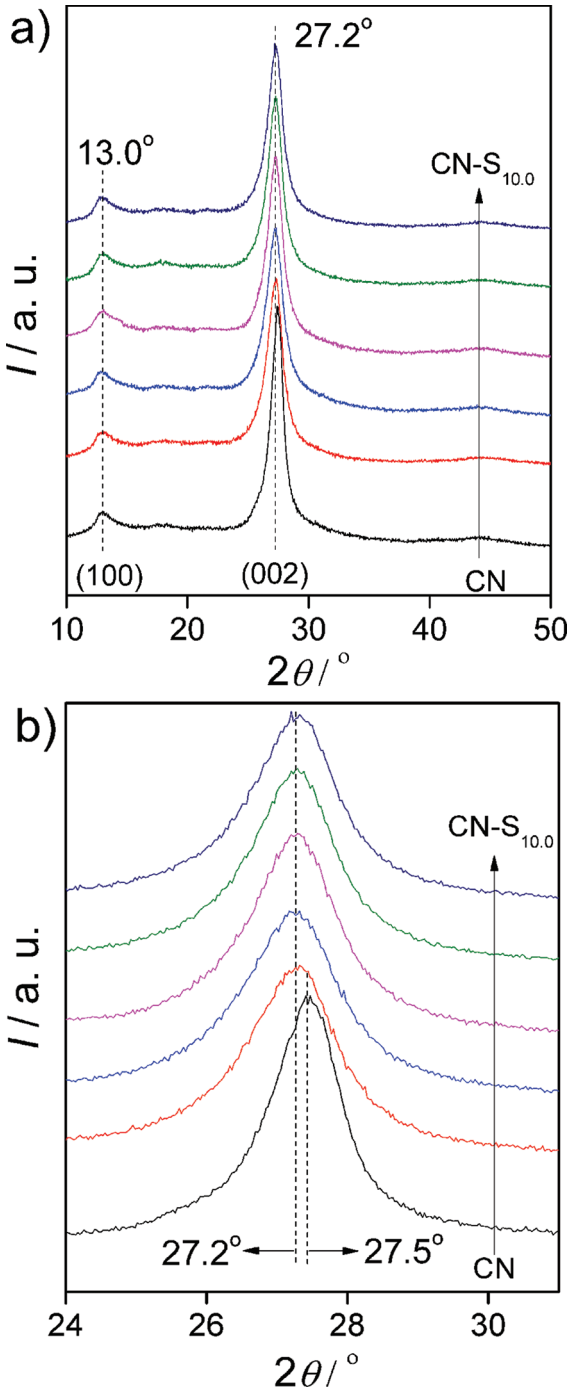

Figure 3. XRD patterns of CN and CN-S_x samples.

1600 cm^{-1} is attributed to the stretching vibration of CN heterocycles; whereas, the sharp peak at 802 cm^{-1} is always recognized as the typical breathing vibration of triazine units. The broad band located in 2900−3300 cm^{-1} is related to residual N−H components and O−H bands, associated with uncondensed amino groups and surface-absorbed H_2O molecules. In comparison with unmodified CN, the vibrations of CN-S_x are less intensive with increasing the amount of S_8, especially for the broad band at 2900−3300 cm^{-1}. The weak band at 2900−3300 cm^{-1} indicates the decrease of uncondensed amino groups in the final samples, demonstrating the accelerated and improved condensation of g-C_3N_4 through sulfur-mediated synthesis.[68] Thus, the S_8-mediated synthesis is

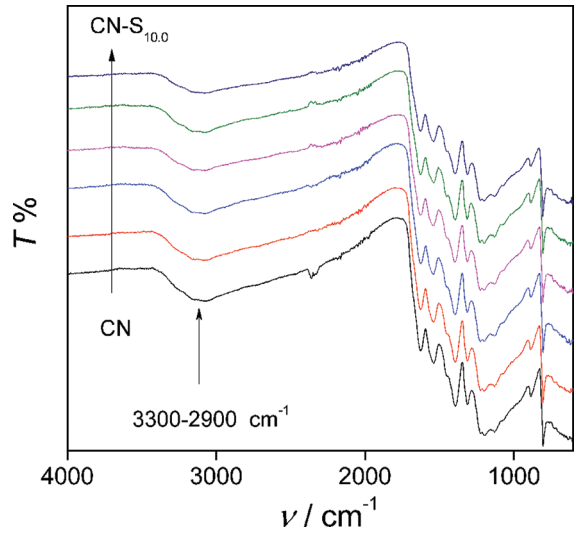

Figure 4. FTIR spectra of CN and CN-S_x samples.

helpful to advance the polymerization of melamine precursor, with less amino-containing groups as surface defects.

The resulting CN-S_x samples were further characterized by XPS to reveal their chemical composition and oxidation state. There are only three elements (C, N, O) detected in the XPS survey spectra of CN-S_x (Figure 5a), almost the same as that of unmodified CN. No other signals assigned to sulfur species can be found, even at the highest S_8 mediated sample CN-$S_{10.0}$. The absence of sulfur species in the resulting CN-S_x is further confirmed by the corresponding high-resolution spectra of S_{2p} with carefully repeated scanning (Figure 5d) and elemental analysis (EA). Thus, the mixture of S_8 with the starting materials is demonstrated to mediate the g-C_3N_4 polymerization instead of doping sulfur in the carbon nitride semiconductors. The O_{1s} peak presented in g-C_3N_4 is presumably due to the surface absorbed H_2O or CO_2 molecules, as confirmed by the above FT-IR analysis (Figure 4). The structure details about backbone C and N elements in g-C_3N_4 were further investigated by their corresponding high-resolution spectra. There are mainly two carbon species presented in the C_{1s} spectra (Figure 5b): one (284.6 eV) is sp^2 C—C bonds, and the other one (288.0 eV) is sp^2-hybridized carbon in N-containing aromatic ring (N—C═N). The latter is considered as the major carbon species in polymeric g-C_3N_4. In Figure 5c, four peaks are deconvoluted for N_{1s} spectra. The highest peak centering at 398.5 eV is regarded as the sp^2-hybridized nitrogen involved in triazine rings (C—N═C), whereas the peak at 400.1 eV corresponds to the tertiary nitrogen N—$(C)_3$ groups. Both of them, together with sp^2-hybridized carbon (N—C═N, 288.0 eV) compose the heptazine heterocyclic ring unites, constructing the basic substructure units of g-C_3N_4 polymers. The weak peak at 401.2 eV indicates the presence of amino functions (C—N—H), originating from the incomplete condensation of poly(tri-*s*-triazine) structures. A careful examination reveals that the peak at 401.2 becomes less intensive with increasing S_8 content, again demonstrating the accelerated and improved effect of sulfur-mediated synthesis for g-C_3N_4 polymerization, in good agreement with the above FTIR analysis (Figure 4). The last peak at 404.1 eV is attributed to charging effects or positive charge localization in heterocycles.

dx.doi.org/10.1021/cs300167b | *ACS Catal.* 2012, 2, 940−948

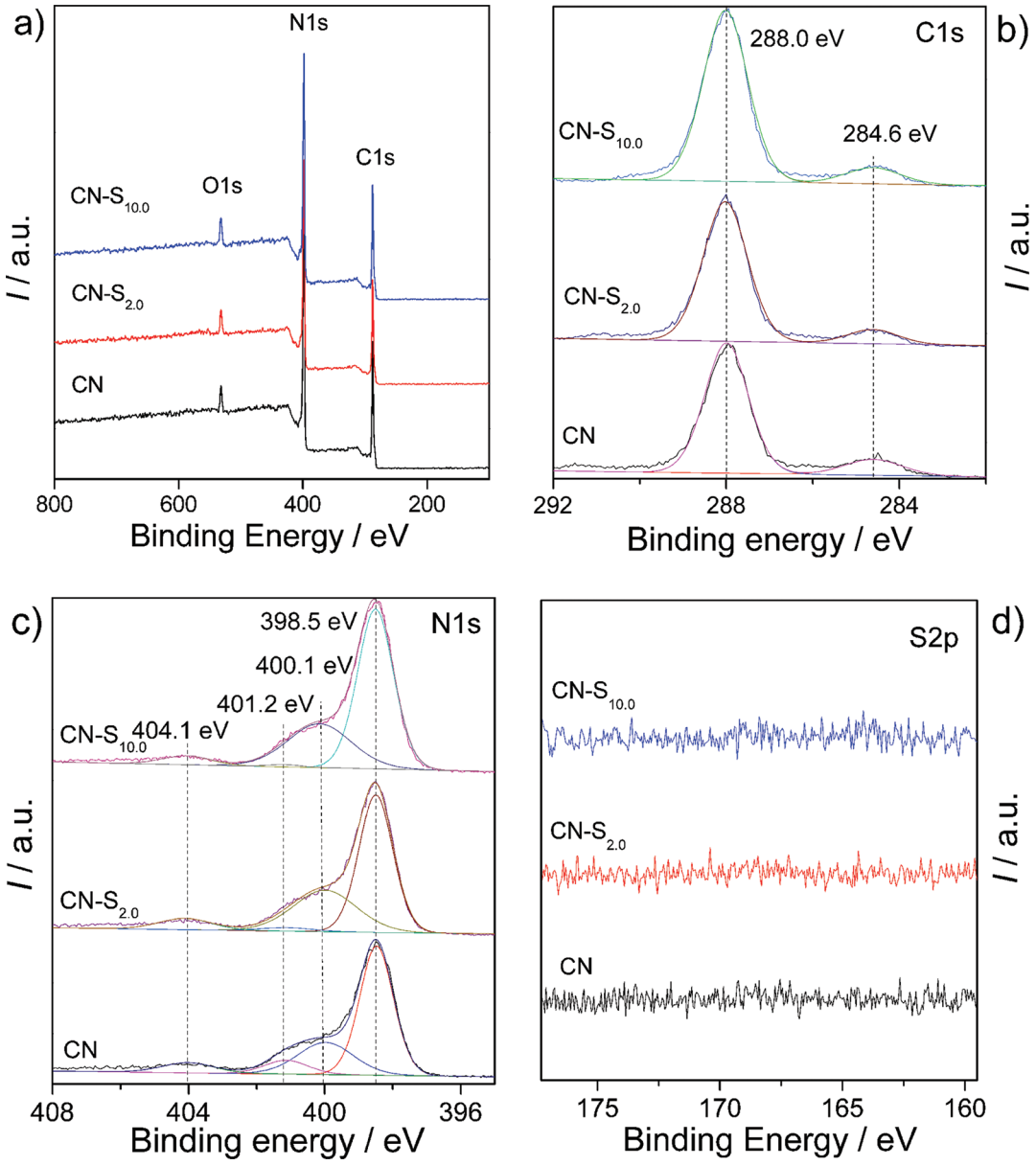

Figure 5. XPS spectra of CN, CN-$S_{2.0}$, and CN-$S_{10.0}$.

Thermogravimetric analysis (TGA) was carried out to evaluate the thermal stability of carbon nitride polymers. As shown in Figure 6, the thermal performance of S_8 modified sample is quite different from that of unmodified CN. The first mass loss happened below 260 °C is due mainly to the volatilization of absorbed H_2O or other volatile impurities on the sample surface. Further increasing heating temperature causes the decomposition of g-C_3N_4, chemically converting carbon nitride into carbon and nitrogen containing gases. The onset temperature of thermal decomposition for CN-$S_{2.0}$ is detected as 510 °C, around 20 °C lower than that for unmodified CN. The complete weight loss of CN-$S_{2.0}$ finishes at 690 °C, 30 °C ahead of that for CN. Thus, the S_8-mediated synthesis slightly decreases the thermal stability of carbon nitride polymers, potentially due to the altered local packing motifs with decreased nanoparticle size.

The electronic properties of CN-S_x were first characterized by the room-temperature EPR spectra. In Figure 7, a single Lorentzian line centering at a *g* value of 2.0034 is presented for all g-C_3N_4 samples. These Lorentzian lines, according to the literature,[51,57] are ascribed to the unpaired electrons on aromatic rings of atoms, within π bonded nanosized clusters. The intensity of Lorentzian lines increases step by step with increasing S_8 amount in the starting materials, indicating the progressive development of electronic band structure promoted by the sulfur flux medium.

The optical features and electronic band gaps of CN-S_x samples were also examined, together with CN as a reference. As shown in Figure 8, a typical semiconductor absorption in the blue region is observed for all CN-S_x samples, indicating the development of semiconductor band structures. Density functional theory (DFT) calculations suggest that the visible-light response of g-C_3N_4 originates from electron transition from the valence band (VB) populated by N_{2p} orbitals to the conduction band (CB) formed by C_{2p} orbitals.[34,35] Thus, the optical properties and semiconductor band structure of g-C_3N_4 polymers can be easily modified by sulfur-mediated synthesis through altering the packing style of π-conjugated aromatic

dx.doi.org/10.1021/cs300167b | *ACS Catal.* 2012, 2, 940−948

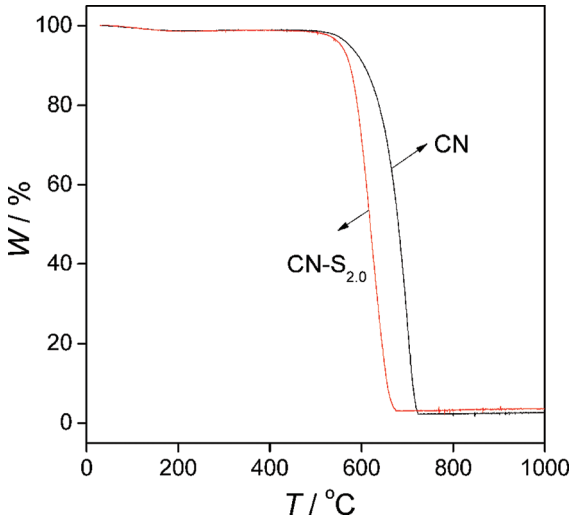

Figure 6. TGA curves of CN and CN-$S_{2.0}$ in air at a heating rate of 5 K min^{-1}.

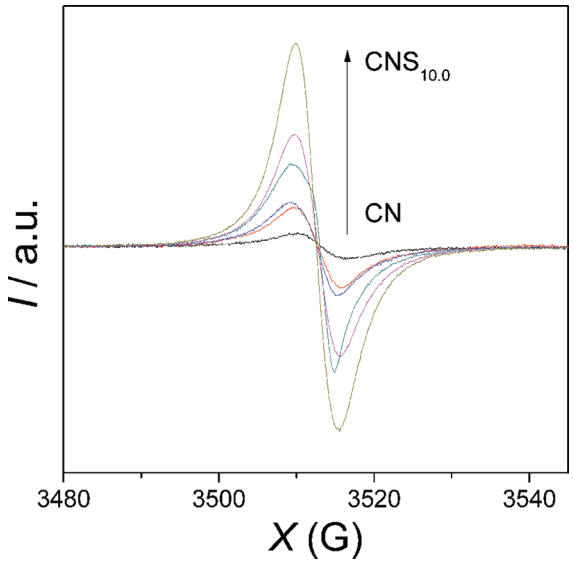

Figure 7. EPR spectra of CN and CN-S_x samples in the dark.

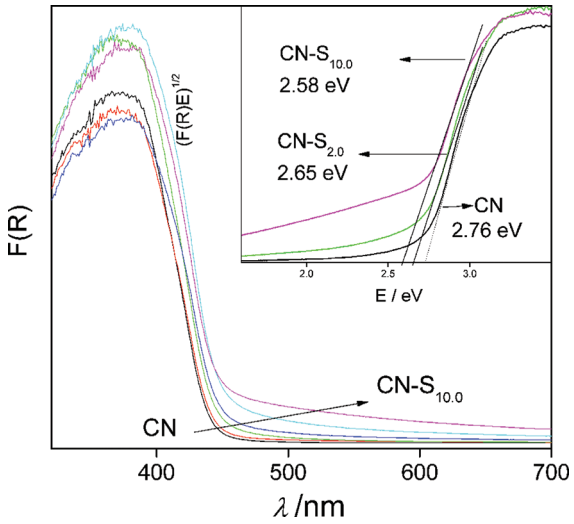

Figure 8. Ultraviolet−visible spectra and corresponding Tauc plot (inset) for CN and CN-S_x samples.

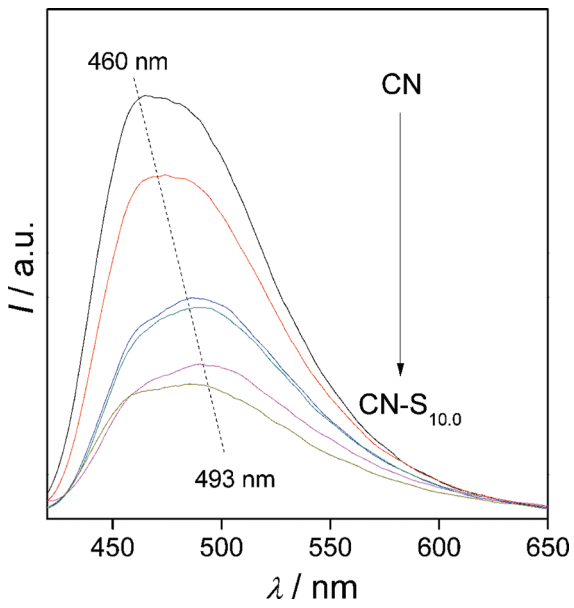

Figure 9. PL spectra under 400 nm excitation for CN and CN-S_x.

systems in g-C_3N_4 semiconductors.[51] As a result of the sulfur-mediated function, the absorption edge of CN-S_x semiconductors is gradually red-shifted with increasing S_8 amount. For example, the absorption edge for unmodified CN is ~450 nm, while after S_8-medaited synthesis it shifts to a longer wavelength of ~480 nm for CN-$S_{10.0}$. The corresponding band gaps (estimated from the absorption edge using the Tauc plot) of CN and CN-S_x are summarized in Table 1. Moreover, an additional adsorption extending to longer wavelength is observed for all CN-S_x samples, due to the intermediate energy levels related to the structural imperfection/surface defects induced by sulfur-mediated synthesis.[72,73]

Photoluminescence (PL) spectra originated from radiative recombination of charge carriers (electron−hole pairs) were further conducted to investigate the optical and electronic properties of CN-S_x.[37,46,51] In Figure 9, a strong PL peak is detected for all g-C_3N_4 samples at room temperature, indicating the generation and recombination of photoinduced charge carriers within carbon nitride semiconductors excited by 400 nm light. An obvious fluorescence quenching is observed for CN-S_x, indicating that the radiative charge recombination which happened on the g-C_3N_4 polymer has been efficiently suppressed after S_8-mediated synthesis, due to the optimized textural structure and electronic properties that facilitates charge separation.[50,51] Radiationless transitions have also been considered to cause fluorescence quenching, which is an unwanted process in photocatalysis either, increasing heat loss. Furthermore, a slight red-shift of fluorescence emission peak from 460 to 493 nm is detected, due to bandgap narrowing effect associated with the S_8-mediated synthesis.[51]

The generation of photoinduced electron−hole pairs, as well as their separation, migration and capture by reactive species, is regarded as the basic process for the operation of semiconductor photocatalysts. Photoelectrochemistry provides us a powerful tool to monitor these complicated processes, and therefore, the powder CN and CN-S_x were made as film electrodes onto fluorine doped tin oxide (FTO) glass.[50,51] Then, these working electrodes were operated in a conventional three electrode cell, with platinum foil and Ag/AgCl as

dx.doi.org/10.1021/cs300167b | ACS Catal. 2012, 2, 940−948

the counter electrode and reference electrode, respectively. In Figure 10, a stable cathode photocurrent is generated by the g-

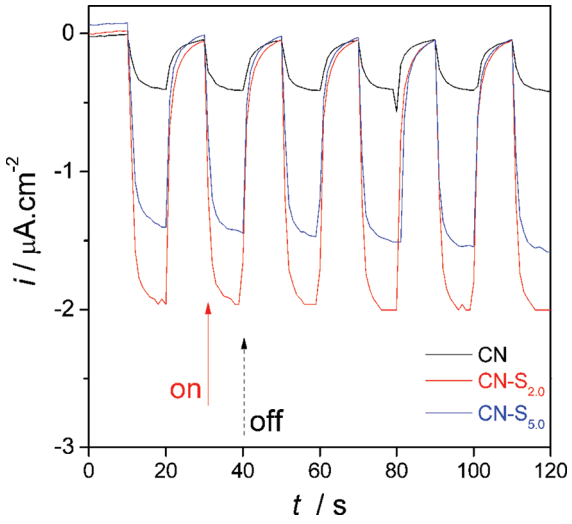

Figure 10. Transient photocurrent response of CN and CN-S_x samples at −0.2 V vs Ag/AgCl in 0.2 M Na_2SO_4 under visible light irradiation (λ > 420 nm, 300 W Xe lamp).

C_3N_4 photoelectrode at −0.2 V vs Ag/AgCl under visible light irradiation (λ > 420 nm), suggesting the generation and separation of electron−hole pairs within semiconductor/electrolyte interfaces and the subsequent redox reactions. As expected, a much enhanced photocurrent is generated by the CN-S_x photoelectrode over the unmodified CN sample, due to the improved efficiency of charge separation (Figure 9) and the enlarged surface area with smaller particle size (Figure 2). The slight photocurrent responded at CN-$S_{5.0}$ is presumably caused by the increase of additional energy levels within electronic band structures, which is considered to capture the charge carriers to stop the subsequent redox reactions. Thus, based on the improved photocurrent performance, a better photocatalytic activity can be envisaged.

The photocatalytic performance of CN-S_x samples was first evaluated by photocatalytic hydrogen evolution under visible light irradiation, using triethanolamine as a sacrificial agent. In our reaction system, chloroplatinic acid ($H_2PtCl_6{\cdot}6H_2O$) was used as the Pt precursor to in situ photodeposit proton reduction sites, whereas triethanolamine was employed as the sacrificial electrons donor for H_2 evolution.[34] As shown in Figure 11a, all CN-S_x samples show an improved H_2 evolution activity over unmodified CN catalyst, underlining the advantage of sulfur-mediated synthesis of g-C_3N_4 photocatalysts. The activity obtained at CN-$S_{2.0}$ is about 5 times higher than that of unmodified sample CN, owing to the optimized textural, optical, and electronic properties. Moreover, the H_2 evolution activity is rather stable that no obvious deactivation is detected after 16 h of continuous irradiation (Figure 11b). The steady increase of H_2 gas with prolonged time of light irradiation, together with the conclusion of the controlled experiment that no gas was produced in the dark, confirms the fact that H_2 is indeed produced by visible light induced electrons transitioning from VB to CB.

Photocatalytic water oxidation is regarded as a crucial step in a series of photosynthetic reactions.[34,35,37,55] Tremendous efforts have been devoted to overcoming this key bottleneck of water splitting chemistry. Until now, there is rare progress

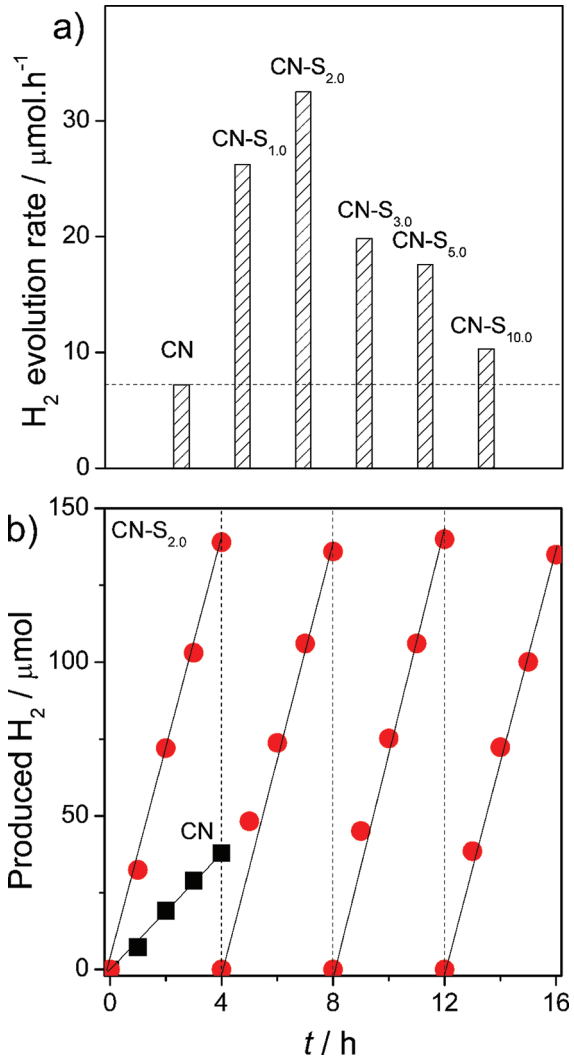

Figure 11. (a) Hydrogen evolution rates based on CN and CN-S_x photocatalysts. (b) Hydrogen-evolution by CN and CN-$S_{2.0}$ as a function of time.

reported for g-C_3N_4 photocatalysts in water oxidation reaction. Recently, we had demonstrated that sulfur-mediated synthesis can provide a chemical tool to control the formation of graphitic carbon nitride, optimizing its photocatalytic ability for water oxidation.[55] In this study, using elemental sulfur (S_8) to replace trithiocyanuric acid, the sulfur-mediated synthesis still works. In Figure 12, a moderate enhancement of O_2 evolution is obtained at CN-S_x photocatalyst, in comparison with unmodified CN. Meanwhile, the selectivity of photogenerated hole is also improved toward water oxidation rather than self-oxidation of the carbon nitride photocatalysts.[37] This is indeed demonstrated by the decrease of N_2 production by CN-S_x. Further modification of CN-S_x to promote catalytic water oxidation kinetic of carbon nitride polymers is ongoing now, such as by joining CN-S_x with oxygen evolution catalyst or by hybridizing CN-S_x with other type of photocatalyst to promote charge separation.

4. CONCLUSIONS

We have demonstrated that using elemental sulfur, as the external sulfur species to act as the chemical promoter for g-C_3N_4 synthesis, can significantly alter the traditional polymer-

dx.doi.org/10.1021/cs300167b | ACS Catal. 2012, 2, 940−948

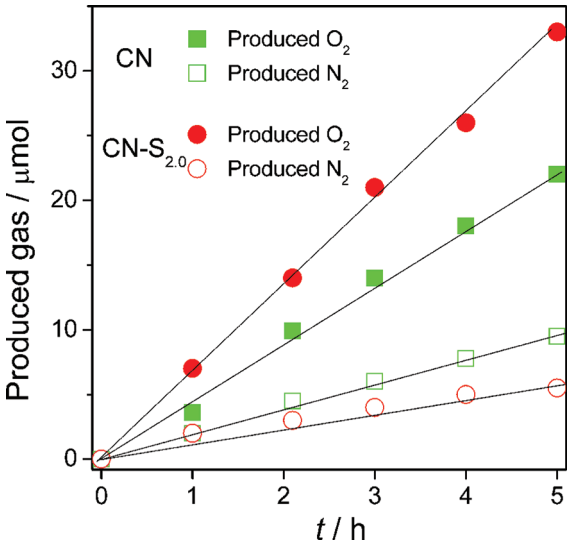

Figure 12. Oxygen-evolution by CN and CN-$S_{2.0}$ as a function of reaction time.

ization route of carbon nitride, improving its intrinsic texture, morphology, optical, and electronic properties for photocatalytic water reduction and oxidation reactions with visible light irradiation. This offers a simple but economic and powerful tool to control the generation of carbon nitride polymers, which can be envisaged to combine with the developed modification protocols of carbon nitride polymers to further modify the sulfur-flux-mediated carbon nitride semiconductors for green catalysis and visible light photocatalysis mainly based on the earth-rich elements, carbon, and nitrogen.[74,75]

AUTHOR INFORMATION

Corresponding Author

*E-mail: xcwang@fzu.edu.cn.

Notes

The authors declare no competing financial interest.

ACKNOWLEDGMENTS

This work is financially supported by the National Natural Science Foundation of China (21033003 and 21173043).

REFERENCES

(1) Dempsey, J. L.; Esswein, A. J.; Manke, D. R.; Rosenthal, J.; Soper, J. D.; Nocera, D. G. *Inorg. Chem.* **2005**, *44*, 6879.
(2) Mccormack, M. *Chem. Eng. News.* **1999**, *77*, 3.
(3) Miller, S. *Environ. Sci. Technol.* **1983**, *17*, 75.
(4) Nechodom, M.; Schuetzle, D.; Ganz, D.; Cooper, J. *Environ. Sci. Technol.* **2008**, *42*, 13.
(5) Su, D. S.; Zhang, J.; Frank, B.; Thomas, A.; Wang, X.; Paraknowitsch, J.; Schlögl, R. *ChemSusChem* **2010**, *3*, 169.
(6) Lewis, N. S.; Nocera, D. G. *Proc. Natl. Acad. Sci. U.S.A.* **2006**, *103*, 15729.
(7) Wolf, M. *Science* **1974**, *184*, 38.
(8) Ginley, D.; Green, M. A.; Collins, R. *MRS Bulletin.* **2008**, *33*, 355.
(9) Crabtree, G. W.; Lewis, N. S. *Phys. Today* **2007**, *60*, 37.
(10) Navarro, R. M.; Peña, M. A.; Fierro, J. L. G. *Chem. Rev.* **2007**, *107*, 3952.
(11) Hains, A. W.; Liang, Z. Q.; Woodhouse, M. A.; Gregg, B. A. *Chem. Rev.* **2010**, *110*, 6689.
(12) Hochbaum, A. I.; Yang, P. D. *Chem. Rev.* **2010**, *110*, 527.
(13) Chen, X. B.; Shen, S. H.; Guo, L. J.; Mao, S. S. *Chem. Rev.* **2010**, *110*, 6503.
(14) Kudo, A.; Miseki, Y. *Chem. Soc. Rev.* **2009**, *38*, 253.
(15) Osterloh, F. E. *Chem. Mater.* **2008**, *20*, 35.
(16) Maeda, K.; Domen, K. *J. Phys. Chem .C* **2007**, *111*, 7851.
(17) Wang, X.; Maeda, K.; Lee, Y.; Domen, K. *Chem. Phys. Lett.* **2008**, *457*, 134.
(18) Fujishima, A.; Honda, K. *Nature* **1972**, *238*, 37.
(19) Asahi, R.; Morikawa, T.; Ohwaki, T.; Aoki, K.; Taga, Y. *Science* **2001**, *293*, 269.
(20) Hosogi, Y.; Tanabe, K.; Kato, H.; Kobayashi, H.; Kudo, A. *Chem. Lett.* **2004**, *33*, 28.
(21) Chen, Y.; Li, D.; Wang, X.; Wang, X.; Fu, X. *Chem. Commun.* **2004**, 2304.
(22) Huang, J.; Ding, K.; Hou, Y.; Wang, X.; Fu, X. *ChemSusChem* **2008**, *1*, 1011.
(23) Maeda, K.; Teramura, K.; Lu, D. L.; Takata, T.; Saito, N.; Inoue, Y.; Domen, K. *Nature* **2006**, *440*, 295.
(24) Maeda, K.; Domen, K. *MRS Bull.* **2010**, *36*, 25.
(25) Tsuji, I.; Kato, H.; Kobayashi, H.; Kudo, A. *J. Am. Chem. Soc.* **2004**, *126*, 13406.
(26) Wang, X.; Maeda, K.; Lee, Y.; Domen, K. *Chem. Phys. Lett.* **2008**, *457*, 134.
(27) Ohwaki, T.; Aoki, K.; Taga, Y. *Science* **2001**, *293*, 269.
(28) Chen, X.; Wang, X.; Hou, Y.; Huang, J.; Wu, L.; Fu, X. *J. Catal.* **2008**, *255*, 59.
(29) Zhao, L.; Chen, X.; Wang, X.; Zhang, Y.; Wei, W.; Sun, Y.; Antonietti, M.; Titirici, M. *Adv. Mater.* **2010**, *22*, 3317.
(30) Ding, Z.; Huang, J.; Wang, X. *Phys. Chem. Chem. Phys.* **2010**, *12*, 5983.
(31) Maeda, K.; Domen, K. *J. Phys. Chem. Lett.* **2010**, *1*, 2655.
(32) Liu, A. Y.; Cohen, M. L. *Science* **1989**, *245*, 841.
(33) Molina, B.; Sansores, L. E. *Modern Phys. Lett. B* **1999**, *13*, 193.
(34) Wang, X.; Maeda, K.; Thomas, A.; Takanabe, K.; Xin, G.; Carlsson, J. M.; Domen, K.; Antonietti, M. *Nat. Mater.* **2009**, *8*, 76.
(35) Maeda, K.; Wang, X.; Nishihara, Y.; Lu, D.; Antonietti, M.; Domen, K. *J. Phys. Chem. C* **2009**, *113*, 4940.
(36) Di, Y.; Wang, X.; Thomas, A.; Antonietti, M. *ChemCatChem* **2010**, *2*, 834.
(37) Zhang, J.; Grzelczak, M.; Hou, Y.; Maeda, K.; Domen, K.; Fu, X.; Antonietti, M.; Wang, X. *Chem. Sci.* **2011**, *3*, 443.
(38) Wang, X.; Chen, X.; Thomas, A.; Fu, X.; Antonietti, M. *Adv. Mater.* **2009**, *21*, 1609.
(39) Chen, X.; Zhang, J.; Fu, X.; Antonietti, M.; Wang, X. *J. Am. Chem. Soc.* **2009**, *131*, 11658.
(40) Ding, Z.; Chen, X.; Antonietti, M.; Wang, X. *ChemSusChem* **2011**, *4*, 274.
(41) Liu, G.; Niu, P.; Sun, C.; Smith, S. C.; Chen, Z.; Lu, G. Q. (Max); Cheng, H. *J. Am. Chem. Soc.* **2010**, *132*, 11642.
(42) Zhang, Y.; Mori, T.; Ye, J.; Antonietti, M. *J. Am. Chem. Soc.* **2010**, *132*, 6294.
(43) Zhang, Y.; Mori, T.; Niu, L.; Ye, J. *Energy Environ. Sci.* **2011**, *4*, 4517.
(44) Zhang, Y.; Thomas, A.; Antonietti, M.; Wang, X. *J. Am. Chem. Soc.* **2009**, *131*, 50.
(45) Takanabe, K.; Kamata, K.; Wang, X.; Antonietti, M.; Kubota, J.; Domen, K. *Phys. Chem. Chem. Phys.* **2010**, *12*, 13020.
(46) Wang, X.; Maeda, K.; Chen, X.; Takanabe, K.; Domen, K.; Hou, Y.; Fu, X.; Antonietti, M. *J. Am. Chem. Soc.* **2009**, *131*, 1680.
(47) Chen, X.; Jun, Y.; Takanabe, K.; Maeda, K.; Domen, K.; Fu, X.; Antonietti, M.; Wang, X. *Chem. Mater.* **2009**, *21*, 4093.
(48) Li, X.; Zhang, J.; Chen, X.; Fischer, A.; Thomas, A.; Antonietti, M.; Wang, X. *Chem. Mater.* **2011**, *23*, 4344.
(49) Kailasam, K.; Epping, J. D.; Thomas, A.; Losse, S.; Junge, H. *Energy Environ. Sci.* **2011**, *4*, 4668.
(50) Zhang, J.; Chen, X.; Takanabe, K.; Maeda, K.; Domen, K.; Epping, J. D.; Fu, X.; Antonietti, M.; Wang, X. *Angew. Chem., Int. Ed.* **2010**, *49*, 441.

(51) Zhang, J.; Zhang, G.; Chen, X.; Lin, S.; Möhlmann, L.; Dolega, G.; Lipner, G.; Antonietti, M.; Blechert, S.; Wang, X. *Angew. Chem., Int. Ed.* **2012**, *51*, 3183.
(52) Li, G.; Yang, N.; Wang, W.; Zhang, W. *J. Phys. Chem. C.* **2009**, *113*, 14829.
(53) Ang, T. P. *Catal. Commun.* **2009**, *10*, 1920.
(54) Yan, S.; Lu, S.; Li, Z.; Zou, Z. *Dalton Trans.* **2010**, *39*, 1488.
(55) Zhang, J.; Sun, J.; Maeda, K.; Domen, K.; Liu, P.; Antonietti, M.; Fu, X.; Wang, X. *Energy Environ. Sci.* **2010**, *4*, 675.
(56) Cui, Y.; Zhang, J.; Zhang, G.; Huang, J.; Liu, P.; Antonietti, M.; Wang, X. *J. Mater. Chem.* **2011**, *21*, 13032.
(57) Zhang, G.; Zhang, J.; Zhang, M.; Wang, X. *J. Mater. Chem.* **2012**, *22*, 8083.
(58) *Mineral Commodity Summaries*, US Geological Survey: Reston, VA, 2009; p 160.
(59) Bacon, R. F.; Fanelli, R. *J. Am. Chem. Soc.* **1943**, *65*, 639.
(60) Fanelli, R. *J. Am. Chem. Soc.* **1945**, *67*, 1832.
(61) He, X.; Wang, L.; Pu., W.; Ren, J.; Wu, W.; Jiang, C.; Wan, C. *J. Therm. Anal. Calorim.* **2008**, *94*, 151.
(62) Currell, B. R.; Williams, A. J. *Thermochim. Acta* **1974**, *9*, 255.
(63) Helton, M. E.; Chen, P.; Paul, P. P.; Tyeklár, Z.; Sommer, R. D.; Zakharov, L. N.; Rheingold, A. L.; Solomon, E. I.; Karlin, K. D. *J. Am. Chem. Soc.* **2003**, *125*, 1160.
(64) Yin, Y.; Rioux, R. M.; Erdonmez, C. K.; Hughes, S.; Somorjai, G. A.; Alivisatos, A. P. *Science* **2004**, *304*, 711.
(65) Yin, Y.; Erdonmez, C. K.; Cabot, A.; Hughes, S.; Alivisatos, A. P. *Adv. Funct. Mater.* **2006**, *16*, 1389.
(66) Li, Z.; Ji, Y.; Xie, R.; Grisham, S. Y.; Peng, X. *J. Am. Chem. Soc.* **2011**, *133*, 17248.
(67) Chung, W. J.; Simmonds, A. G.; Griebel, J. J.; Kim, E. T.; Suh, H. S.; Shim, I.; Glass, R. S.; Loy, D. A.; Theato, P.; Sung, Y. *Angew. Chem., Int. Ed.* **2011**, *50*, 11409.
(68) Bojdys, M. J.; Müller, J.; Antonietti, M.; Thomas, A. *Chem.—Eur. J.* **2008**, *14*, 8177.
(69) Dubois, P.; Lelieur, J. P.; Lepoutre, G. *Inorg. Chem.* **1989**, *28*, 195.
(70) Chun, W. J.; Ishikawa, A.; Fujisawa, H.; Takata, T.; Kondo, J. N.; Hara, M.; Kawai, M.; Matsumoto, Y.; Domen, K. *J. Phys. Chem. B* **2003**, *107*, 1798.
(71) Hitoki, G.; Ishikawa, A.; Takata, T.; Kondo, J. N.; Hara, M.; Domen, K. *Chem. Lett.* **2002**, 736.
(72) Queisser, H. J.; Haller, E. E. *Science* **1998**, *281*, 945.
(73) Chen, X.; Liu, L.; Yu, P. Y.; Mao, S. S. *Science* **2011**, *331*, 746.
(74) Su, F.; Mathew, S. C.; Möhlmann, L.; Antonietti, M.; Wang, X.; Blechert, S. *Angew. Chem., Int. Ed.* **2011**, *50*, 657.
(75) Su, F.; Mathew, S. C.; Lipner, G.; Fu, X.; Antonietti, M.; Blechert, S.; Wang, X. *J. Am. Chem. Soc.* **2010**, *132*, 16299.